

Ultrastructure of Long-Range Transport Carriers Moving from the *trans* Golgi Network to Peripheral Endosomes

Roman S. Polishchuk^{1*}, Enrica San Pietro¹,
Alessio Di Pentima¹, Stefano Teté² and Juan
S. Bonifacino³

¹Department of Cell Biology and Oncology, Consorzio
Mario Negri Sud, 66030, Santa Maria Imbaro (Chieti), Italy

²Department of Oral Sciences, University 'G. D'Annunzio',
66013, Chieti, Italy

³Cell Biology and Metabolism Branch, National Institute of
Child Health and Human Development, National Institutes
of Health, Bethesda, MD 20892, USA

*Corresponding author: polish@dco.negrissud.it

The delivery of mannose 6-phosphate receptors carrying lysosomal hydrolases from the *trans*-Golgi network (TGN) to the endosomal system is mediated by selective incorporation of the receptor–hydrolase complexes into vesicular transport carriers (TCs) that are coated with clathrin and the adaptor proteins, GGA and AP-1. Previous electron microscopy (EM) and biochemical studies have shown that these TCs consist of spherical coated vesicles with a diameter of 60–100 nm. The use of fluorescent live cell imaging, however, has revealed that at least some of this transport relies on a subset of apparently larger and highly pleiomorphic carriers that detach from the TGN and translocate toward the peripheral cytoplasm until they meet with distally located endosomes. The ultrastructure of such long-range TCs has remained obscure because of the inability to examine by conventional EM the morphological details of rapidly moving organelles. The recent development of correlative light-EM has now allowed us to obtain ultrastructural 'snapshots' of these TCs immediately after their formation from the TGN in live cells. This approach has revealed that such carriers range from typical 60- to 100-nm clathrin-coated vesicles to larger, convoluted tubular-vesicular structures displaying several coated buds. We propose that this subset of TCs serve as vehicles for long-range distribution of biosynthetic or recycling cargo from the TGN to the peripheral endosomes.

Key words: clathrin, endosomes, GGAs, long-range transport carriers, TGN

Received 22 December 2005, revised and accepted for publication 18 May 2006

Introduction

Mannose 6-phosphate receptors (MPRs) carrying lysosomal hydrolase precursors are sorted at the *trans*-Golgi

network (TGN) by segregation into membrane domains that are coated with clathrin and the adaptor proteins, GGA and AP-1 (1). These domains give rise to small (60–100 nm diameter) clathrin-coated vesicles (CCVs) that rapidly uncoat and fuse with early or late endosomes, thereby effecting the delivery of MPRs and their cargo enzymes to the endosomal-lysosomal system. Typical CCVs containing MPRs have been observed using electron microscopy (EM) in the vicinity of the TGN (2–4) and have also been isolated and characterized biochemically (5,6). To date, however, they have not been adequately resolved using fluorescence microscopy of living cells because the TGN and endosomes are both concentrated in the juxtannuclear area of the cells, making identification of single CCVs difficult.

Recent fluorescence microscopy studies have uncovered the existence of a different type of transport carrier (TC) containing MPRs, clathrin, GGAs, and/or AP-1. These TCs escape from the juxtannuclear area of the cell and travel long distances (up to 10 μ m) toward the peripheral cytoplasm where they meet with endosomes (7–10). Formation of such TCs coincides with segregation of MPRs from Golgi-resident enzymes and from constitutive cargo directed to the plasma membrane (8–10) and requires the presence of intact microtubules and the Arf1 GTPase (10). These TCs appear under the optical microscope as a pleiomorphic assortment of vesicles and tubules of varying sizes. Their ultrastructure, however, has remained unknown because of the inability to examine the morphology of rapidly moving organelles using conventional EM.

The recent adaptation of correlative light-EM (CLEM) to the study of organelle dynamics now provides an opportunity to examine the ultrastructure of intermediates that mediate transport from the TGN to endosomes. CLEM allows the ultrastructural analysis of moving organelles *in vivo*, typically through the use of protein markers tagged with green fluorescent protein (GFP) variants; the organelles are first identified using fluorescence microscopy and then examined under the electron microscope (11). The potential of this approach has previously been exploited to analyze the ultrastructure of such dynamic organelles as endoplasmic reticulum (ER)-to-Golgi and TGN-to-plasma membrane TCs (12–14).

Here, we report the use of CLEM to demonstrate that GGA1-, clathrin-, and MPR-containing, TGN-derived TCs range from typical CCVs to convoluted tubular-vesicular structures with several coated buds. We propose that

these TCs serve as vehicles for long-range distribution of biosynthetic or recycling cargo from the TGN to peripheral endosomes.

Results

CLEM consists of two steps: (i) identification of an intracellular structure, generally using fluorescence microscopy of live cells that express a marker protein coupled to a GFP variant and (ii) EM of that particular structure, often involving immunolabeling and three-dimensional (3D) reconstruction (12). In effect, this technique can produce high-resolution snapshots of moving organelles, making it ideally suited for the analysis of the ultrastructure of TGN-derived TCs.

To visualize these TCs, we initially transfected HeLa cells with a plasmid encoding GFP-GGA1 and observed the cells under a confocal fluorescence microscope. As previously reported (8,9), this marker protein localized to both a large juxtannuclear cluster (i.e. the TGN) and isolated foci in the peripheral cytoplasm (i.e. peripheral endosomes and TCs) (Figure 1A,B). To distinguish endosomes from TCs, we allowed cells to internalize the fluid-phase marker, TRITC-dextran, for 30 min. GFP-GGA1-positive but TRITC-dextran-negative structures that detached from the juxtannuclear cluster and moved toward the periphery were considered to be TCs. Figure 1A and B (box and inset) and Movie 1 show fluorescent images of three GFP-GGA1-containing TCs, which left the TGN almost simultaneously and moved rapidly toward the periphery. Consistent with previous reports (8,9), these three structures had different appearances. One TC (Figure 1B, arrow) had an elongated shape with two 'hot-spots' at one end, whereas the other two TCs (Figure 1B, open arrow and arrowhead) appeared more compact. None of these structures contained internalized TRITC-dextran (Figure 1B, inset, red), indicating that they were not endosomes. Cells were fixed during the process of live cell imaging, stained with anti-GFP antibody using a pre-embedding immunogold protocol, embedded in resin, and sectioned for EM (12). Correlation of fluorescence and EM images (compare Figure 1B and C) allowed us to find in serial sections all three TCs (Figures 1D and 2A–D). The largest TC had two coated buds connected to an elongated tubular part (arrow in Figures 1D and 2A–D, and in the 3D reconstruction from serial sections shown in Figure 2H,I), which correlated well with its appearance by fluorescence microscopy (Figure 1B, arrow). In contrast, the smaller, rounder TC had the morphology of a 120-nm-diameter coated vesicle (arrowhead in Figures 1D and 2A–C) as revealed also in the 3D reconstruction (Figure 2H,I, arrowhead). Finally, the third TC exhibited a tubular-saccular morphology (Figure 1D, open arrow) with a coat at the tip of the tubular part (see Figure 2G for a clearer image of this coat). The coats on all three TCs had the typical appearance of clathrin coats (Figure 2E–G),

which was consistent with the function of GGA1 as a clathrin adaptor.

Figure 3A, B, and Movie 2 show examples of two other TCs (arrow and arrowhead), which, in this case, were fixed shortly after their emergence from the TGN (the TGN boundary is indicated by a dashed red line in B and C). The ultrastructure of these TCs was similar to that of the larger structure described above: both contained coated buds (two on one carrier and three on the other) that were connected by short tubular stalks (Figure 3C,D, arrow and arrowhead). Hereafter, we refer to this type of structure as 'grape-like' cluster TCs. Notably, coated buds on grape-like TCs were not restricted to the ends of the structure but were also seen attached to the central portion of the tubules. We analyzed 24 GFP-GGA1-positive TCs by CLEM shortly after their exit from the TGN and assigned them to four shape classes: (i) vesicular, (ii) tubular, (iii) saccular, and (iv) grape-like. Grape-like structures represented the majority (approximately 58%), while small vesicles were a minority (approximately 5%) (see below). The sizes of TCs ranged from 100 nm (vesicles) to 1200 nm (all other structures); the average diameter was 410 ± 95 nm (mean \pm SD). Interestingly, GFP-GGA1 immunolabeling was not restricted to the membrane domains that were covered with putative clathrin-like coats. Other parts of the TCs were also positive for GFP-GGA1 (Figures 1D, 2E,G, and 3C,D), which is consistent with previous EM studies showing the presence of GGA1 on both clathrin-coated and uncoated areas of the TGN (4).

Next, we examined the ultrastructure of TGN-derived TCs carrying a cation-dependent (CD)-MPR-GFP construct (abbreviated MPR-GFP), which serves as a transmembrane marker for the TCs (8,9). In the experiment as shown in Figure 4A, B, and Movie 3, we examined two MPR-GFP-positive (green), TRITC-dextran-negative (color inset, red) structures thus identified as TCs. EM of these TCs (Figure 4C–G) revealed that their ultrastructure was similar to that of GFP-GGA1-labeled TCs. One of these TCs appeared in thin sections as a 350 nm-long tubule with a coated bud on its tip (Figure 4C, arrowhead). Analysis of the other carrier (Figure 4C, arrow) by serial sectioning (Figure 4D,E) and 3D reconstruction (Figure 2F,G) showed that it was 460-nm long and exhibited a typical grape-like morphology with three coated buds. CLEM also allowed us to visualize TGN-derived TCs containing MPR-GFP that approached endosomes loaded with TRITC-dextran, as exemplified in Figure 5A, B, and Movie 4. Similar to the GFP-GGA1-containing TCs, the MPR-GFP-containing TC (Figure 5B, arrow) displayed tubular and coated bud domains (Figure 5C, arrow). The neighboring endosome (Figure 5B, inset, arrowhead) exhibited a vacuolar part (Figure 5C, arrowhead) and a tubular extension where the MPR-GFP was concentrated (Figure 5C). This tubular domain may be formed by the arriving TCs or, alternatively, could be involved in recycling of MPR-GFP back to the TGN, as previously proposed

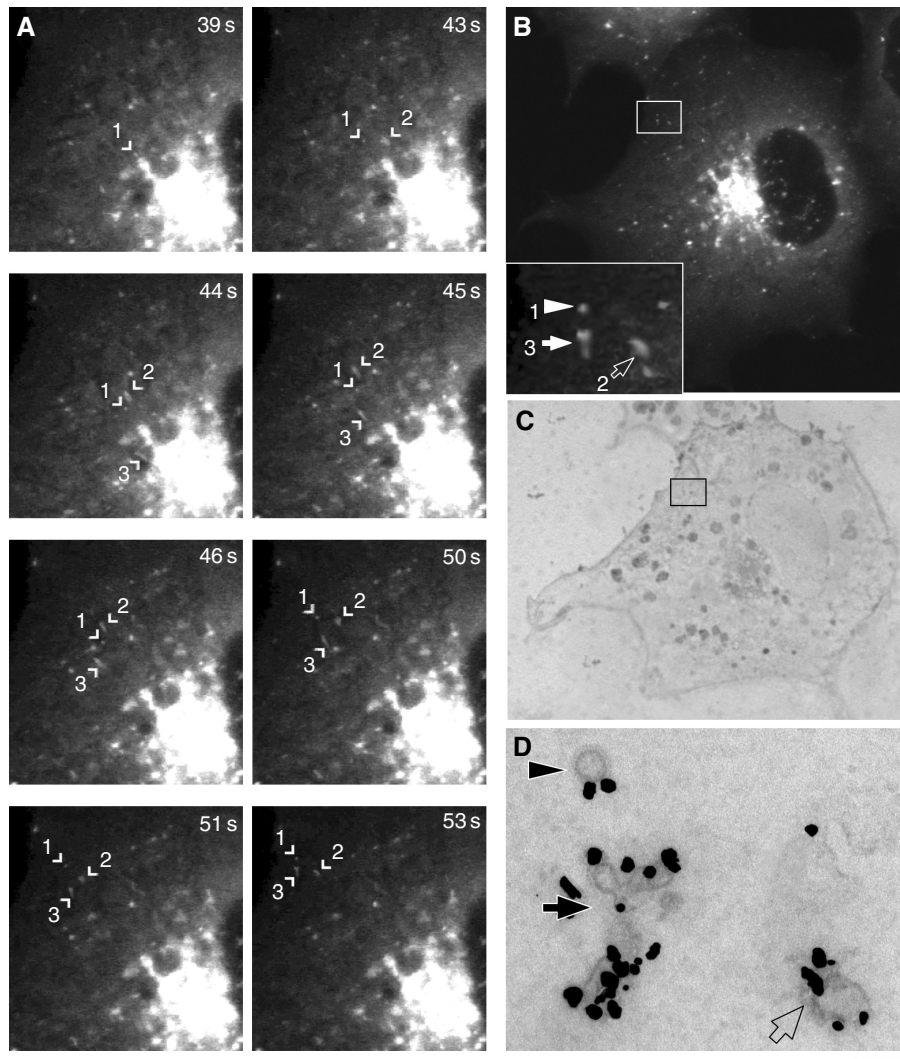


Figure 1: Correlative light-EM (CLEM) of GFP-GGA1-containing TCs. (A) HeLa cells were transfected with a plasmid encoding GFP-GGA1, incubated for 30 min with TRITC-dextran, and imaged using confocal fluorescence microscopy. Sequence of time-lapse frames shows three TCs (arrowheads) that move from the juxtannuclear area in a living cell (see also Movie 1–1). The cell of interest was quickly fixed during the course of observation by addition of a mixture of 4% paraformaldehyde (PFA) and 0.1% glutaraldehyde (GA) to the medium. (B) After fixation, we found again all 3 TCs (indicated by arrows and arrowhead in inset) within the same area of the cell outlined by box. Note the apparent pleiomorphy of the GFP-GGA1-containing TCs (green) and the absence of TRITC-dextran (red) within them. (C) Cells were then prepared for immunogold EM with anti-GFP antibody. Low magnification EM image shows the same cell and the same area (box) as in B. (D) EM of a thin section corresponding to the area indicated by the boxes in panels B, C, and inset in panel B. Cells were immunogold-labeled with antibody to GFP before embedding. The arrow, open arrow, and arrowhead indicate the same three 3 TCs shown in the panel B box and inset. Bar: 3 μ m (A), 4.2 μ m (B, C), 280 nm (D).

(3,15,16). As described above for GFP-GGA1, MPR-GFP molecules were detected on both coated and smooth membrane domains of the TCs. CLEM analysis of 23 MPR-GFP-containing TCs revealed a range of morphologies that was similar to that described above for GFP-GGA1-containing TCs. Also, in this case, grape-like cluster structures accounted for most of the TCs (approximately 57%), while typical coated vesicles were a minority (approximately 5%) (Figure 5D). For both GFP-GGA1-containing and MPR-GFP-containing TCs, 58 and 46%, respectively, of their total surface were coated (Figure 5E).

Because clathrin is a key component of TGN-derived TCs, we next examined by CLEM HeLa cells transfected with a GFP-tagged clathrin light chain (isoform b) construct (herein referred to as clathrin-GFP). Clathrin-GFP was detected in many spots at the plasma membrane and the TGN, as well as throughout the cytoplasm. Some of these clathrin-GFP-containing cytoplasmic structures were observed to arise from the TGN, as previously reported (9). Figure 6 and Movie 5 show one of these TCs that ends its translocation next to a fainter, compact structure at the time of fixation. EM of thin sections showed that

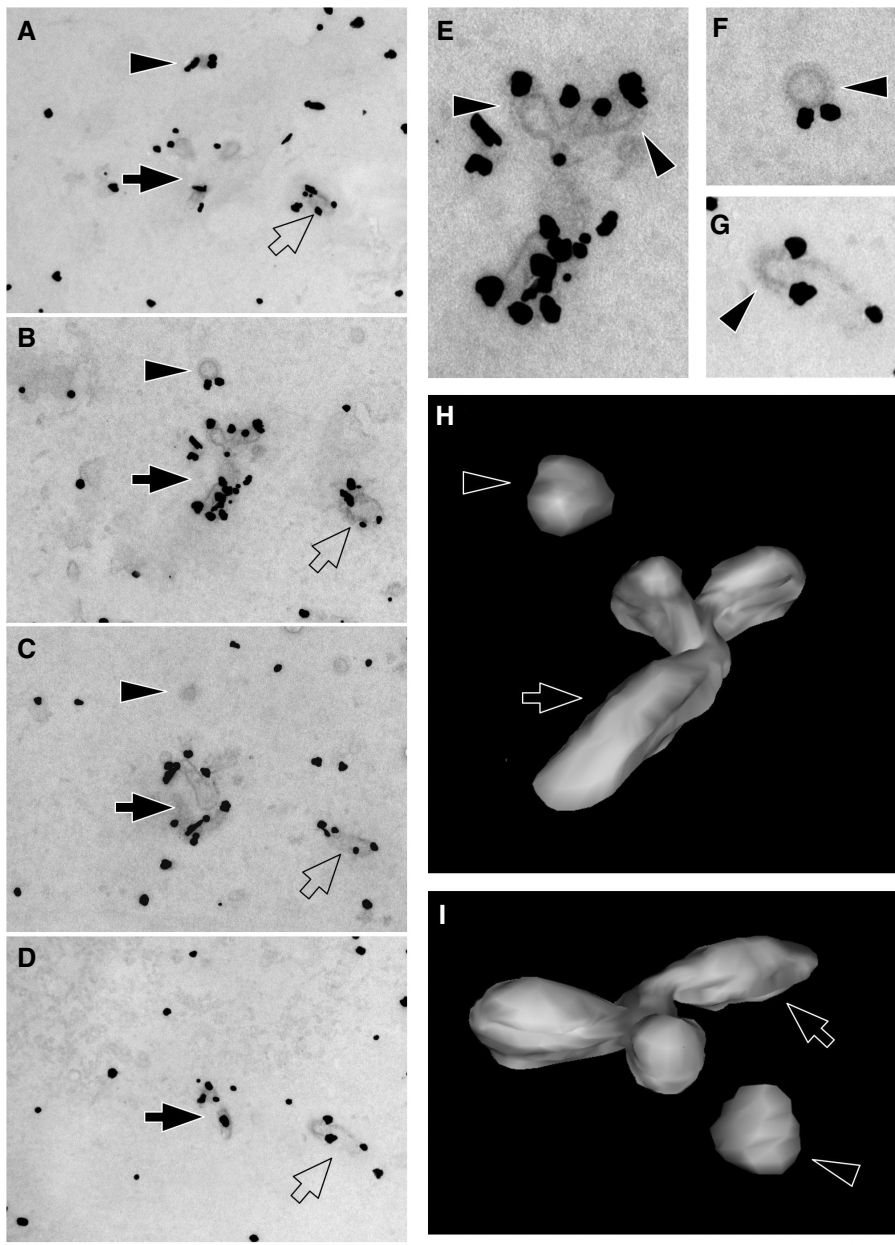


Figure 2: Three-dimensional organization of GFP-GGA1-containing TCs. (A–D) The same 3 TCs shown in Figure 1 were examined in serial sections. (E–G) Arrowheads in high magnification images indicate surface domains of the carriers that are covered by a clathrin coat with characteristic spike-like structures. (H, I) Three-dimensional reconstruction of the GFP-GGA1-containing TCs indicated by the arrow and arrowhead in A–D. Bar: 180 nm (A–D), 350 nm (E–G), 90 nm (H, I).

this TC had a typical grape-like appearance, with two buds that were decorated by gold particles, indicating the presence of clathrin-GFP. The adjacent clathrin-GFP-positive structure was immobile during the course of observation and had the morphology of a typical CCV (Figure 6D, arrowhead); this structure could represent a plasma membrane-associated coated pit or derived vesicle. Analysis of 11 clathrin-GFP-containing TCs using CLEM showed that their ultrastructure was similar to that of the GFP-GGA1-, and MPR-GFP-containing TCs; this was consistent with previous studies demonstrating that all of these proteins co-localize (8,9). The only appreciable difference was that clathrin-GFP labeling was restricted to coated regions of the TCs (see also Figure 8D below),

whereas GFP-GGA1 and MPR-GFP labeling was found on both coated and noncoated areas of the TCs.

Next, we examined whether these TCs maintain their structural properties until they fuse with their target organelles. This is a significant issue because coated buds on other types of TCs are thought to give rise to coated vesicles that recycle molecules back to the donor organelle. For example, COPI-coated buds on ER-to-Golgi TCs have been proposed to generate COPI-coated vesicles that return recycling molecules to the ER (17,18). Likewise, clathrin-coated buds on immature secretory granules are thought to generate CCVs that recycle escaped MPRs to the TGN, thus contributing to granule

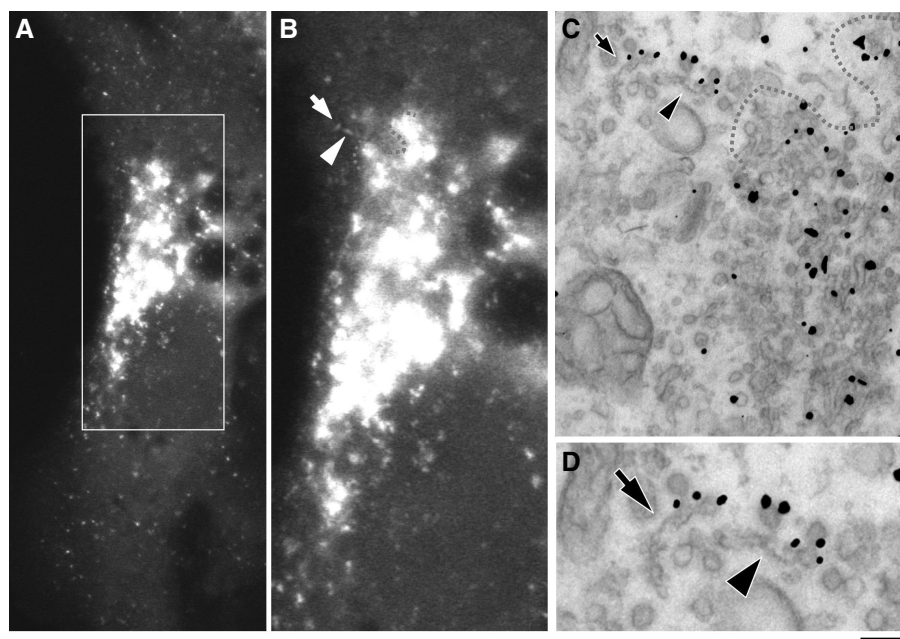


Figure 3: Ultrastructure of GFP-GGA1-containing TCs. (A) A GFP-GGA1-expressing cell was analyzed *in vivo* using time-lapse confocal microscopy (see Movie 1–2). (B) Enlargement of the box shown in A. Two GFP-GGA1-containing TCs (arrow and arrowhead) were fixed near the edge of the Golgi complex (outlined by the dashed red line). (C) Using the Golgi boundary as a landmark (dash line), the same GFP-GGA1-containing TCs (arrow and arrowhead) were identified by EM of thin sections of the cell shown in A, B. (D). High magnification of the GFP-GGA1-containing TCs (arrow and arrowhead), shown in panel C. Bar 3.4 μm (A), 1.7 μm (B), 530 nm (C), 320 nm (D).

maturation (19,20). Clathrin-coated buds on TGN-to-endosome TCs could therefore detach from the carriers as CCVs before the TCs engage in interactions with endosomes. If this were the case, the resulting ‘mature’ TCs would lack coated domains. This is difficult to address using CLEM because one needs to catch TCs in the process of docking or fusing to endosomes. To circumvent this problem, we blocked fusion of TCs with endosomes using the technique of ‘endosome inactivation’ (21–23). MPR-GFP- or GFP-GGA1-expressing HeLa cells were allowed to internalize horseradish peroxidase (HRP) for 1 h and were then incubated with diaminobenzidine (DAB) and H_2O_2 on ice. In this way, the endosomal system of the living cells gets filled up with a rigid DAB oxidation product that prevents fusion of endosomes with other organelles (21–23). The cells were then shifted to 37 °C to allow resumption of TC formation from the TGN. To demonstrate that delivery of cargo from TGN-derived TCs to endosomes was blocked upon endosome inactivation, we used a photobleaching approach on MPR-GFP-expressing cells. In control cells, bleached endosomes recovered their fluorescence because of fusion with TCs carrying MPR-GFP from the TGN (Figure 7A, Movie 6). In contrast, bleaching of inactivated endosomes revealed no such recovery even after 20–30 min of incubation at 37 °C (Figure 7B, Movie 7). TCs were frequently observed to gather in the vicinity of the inactivated endosomes but were apparently unable to fuse with them and to deliver their cargo. Correspondingly, confocal microscopy of

GFP-GGA1-expressing cells showed two to four GFP-GGA1-containing structures gathered around EEA1-positive endosomes 45 min after endosome inactivation (boxes 1–3 in Figure 8A). There was little overlap between the GFP-GGA1 and EEA1 staining, indicating that the GFP-GGA1-containing structures were not endosomes but probably TCs that could not fuse with EEA1-positive endosomes because of accumulation of the DAB oxidation product. At the EM level, we observed many GFP-GGA1-positive TCs (Figure 8B–D) that were tightly associated with HRP-labeled endosomes. As expected, these TCs did not contain DAB oxidation product and exhibited morphologies ranging from short tubules (Figure 8B–D, arrows) and vesicles (Figure 8D, arrowhead) to grape-like clusters (Figure 8D, open arrow). Similar to TCs visualized using CLEM, these carriers exhibited MPR-GFP and GFP-GGA1 over the entire surface (Figure 8B,C), while clathrin-GFP was restricted to the coated domains (Figure 8D).

Quantification of ‘mature TCs’ accumulated upon endosome inactivation revealed a small reduction (about 10%) of grape-like structures in favor of other TCs’ shapes (Figure 8E). In most cases, coats were visible on the TC membranes, although the surface covered by clathrin on mature TCs was slightly reduced (about 12%) relative to TCs analyzed using CLEM (Figure 8F). Thus, the basic ultrastructure of TCs remains mostly unchanged as they translocate from the TGN to the endosomes. The slight reduction of clathrin coats at the TC surface suggests that

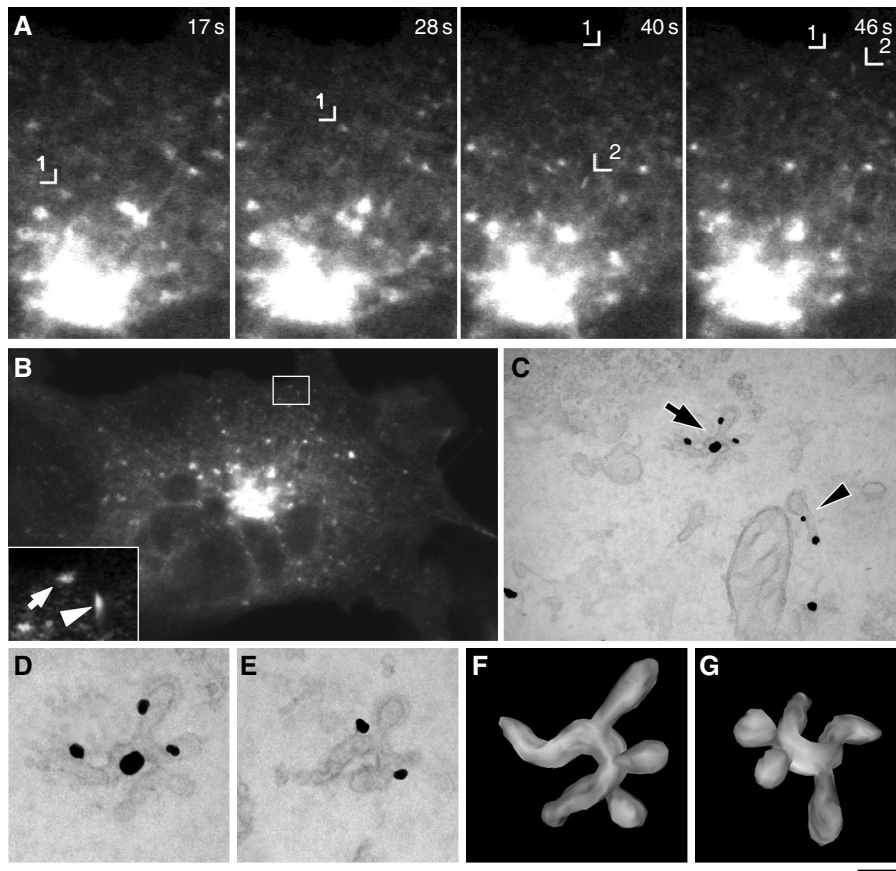


Figure 4: CLEM of MPR-GFP-containing TCs. (A) HeLa cells were transfected with a plasmid encoding MPR-GFP and were incubated for 30 min with TRITC-dextran. Sequence of time-lapse frames shows two TCs (arrowheads) moving from the TGN toward cell periphery (see also Movie 2–1). The cell of interest was quickly fixed during the course of observation by addition of a mixture of 4% PFA and 0.1% GA to the medium. (B) After fixation, both TCs (indicated by arrows and arrowhead in inset) were found again within the same area of the cell outlined by box. Note the lack of MPR-GFP (green) and TRITC-dextran (red) co-localization within the TCs. (C) EM of a thin section corresponding to the area indicated by the box and inset in panel B show the ultrastructure of the same MPR-GFP-containing TCs (arrow and arrowhead) immunogold-labeled with antibody to GFP. (D, E) EM of serial sections showing one of the MPR-GFP-containing TCs (indicated by arrow in C) at higher magnification. (F, G) Three-dimensional reconstruction of the MPR-GFP-containing TC shown in D, E. Bar, 3 μ m (A), 4.8 μ m (B), 350 nm (C), 220 nm (D, E), 170 nm (F, G).

partial uncoating of carriers may take place upon their arrival to the target membrane. To determine whether large TCs form by homotypic fusion of CCVs, we incubated cells with *N*-ethyl maleimide [a general inhibitor of membrane fusion (24)] shortly after endosome inactivation. However, the proportion of CCVs among endosome-directed TCs remained similar to that in control cells (data not shown), suggesting that homotypic CCV fusion does not significantly contribute to the formation of large TCs.

Previous fluorescence microscopy studies suggested that TCs pinch off as whole objects from tubules that extend from the TGN (8,9). Thus, the TGN is likely to contain membrane domains that serve as sources of TCs. Indeed, careful immuno-EM analyses revealed the existence of coated grape-like clusters, labeled for MPR-GFP or GFP-GGA1, in the area of the TGN (Figure 9A, arrows). Both the average size (approximately 400 nm) and the

structural features of these clusters were similar to those of the majority of translocating TCs (Figure 9B,C, arrows). As in the free TCs, clathrin was always restricted to coated membrane domains while both GFP-GGA1 and MPR were detected on both coated and noncoated (usually tubular) domains of the TGN, as previously reported (4). These observations suggest that GGAs may initiate the sequestration of MPRs within tubular areas of the TGN, thus creating a template for TC formation. Interaction of GGAs with clathrin further concentrates MPRs within coated buds until the TCs detach from the bulk of the TGN.

Discussion

Previous fluorescence microscopy analyses had suggested that the TCs that ferry cargo between the TGN

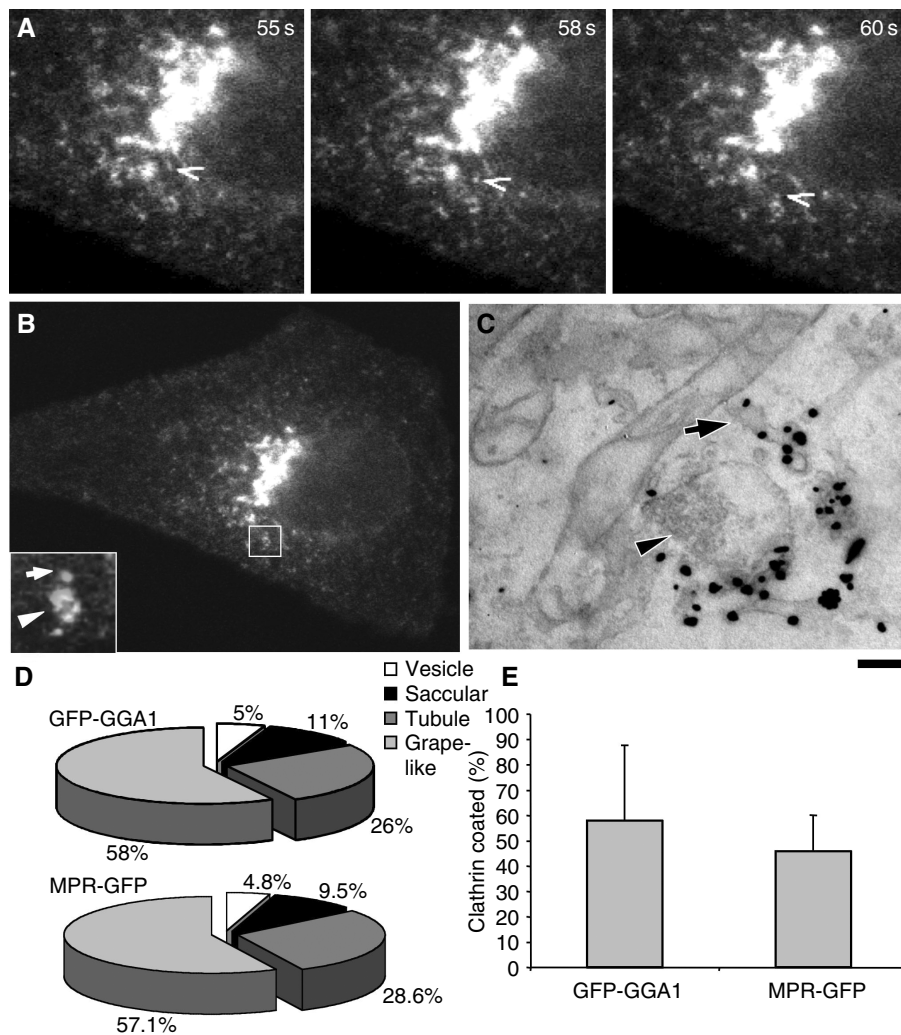


Figure 5: Ultrastructure of MPR-GFP-containing TCs. (A) An MPR-GFP-expressing cell was analyzed *in vivo* using time-lapse confocal microscopy. An MPR-GFP-containing TC (indicated by arrowhead in subsequent time-lapse images) was detected using confocal fluorescence microscopy of a living cell (see also Movie 2–2). (B) An MPR-GFP-containing TC was fixed in the area of the cell outlined by the box. An enlarged image of this area (color inset) shows an MPR-GFP-containing TC (arrow) approaching a TRITC-dextran-loaded endosome (arrowhead). (C) EM of a thin section corresponding to the area indicated by the box and inset in panel B shows the same MPR-GFP-containing TC (arrow) labeled with antibody to GFP next to the endosome (arrowhead). (D) Pie charts representing the frequency of different shapes in populations of GFP-GGA1- and MPR-GFP-containing TCs observed using CLEM. (E) Percentage of area occupied by clathrin coat on the surface of GFP-GGA1- and MPR-GFP-containing TCs. Results are the mean \pm SD from 24 and 23 TCs, respectively. Bar, 3 μ m (A), 5.3 μ m (B), 300 nm (C).

and peripheral endosomes were pleiomorphic but, owing to the low resolution of optical microscopy, had not defined their exact morphology. The use of CLEM has now allowed us to demonstrate that some of the TCs are indeed typical CCVs. To our knowledge, this is the first ultrastructural characterization of translocating CCVs by EM. Importantly, this proves that typical CCVs do exist *in vivo*, that they can be visualized by fluorescence microscopy despite their small size, and that at least some of them move for long distances before shedding their coats. However, most of these TCs consist of tubular-vesicular structures with coated buds that comprise approximately 50% of their surface area. These structures are similar to

TGN domains that contain MPR-GFP and GFP-GGA1 (Figure 9) and might therefore correspond to small ‘chunks’ of TGN that are pulled along microtubules to the cell periphery. The probability of forming a CCV versus a more complex TC probably depends on how soon scission factors act on the necks of the forming TCs after assembly of the coat. The physiological significance of this pleiomorphy is unclear. Presumably, pleiomorphic TCs can package cargoes of different sizes, including those that are too large for inclusion into a CCV. In addition, pleiomorphic TCs might be able to transport simultaneously different types of cargo that partition into coated and noncoated domains of the carriers. The properties of

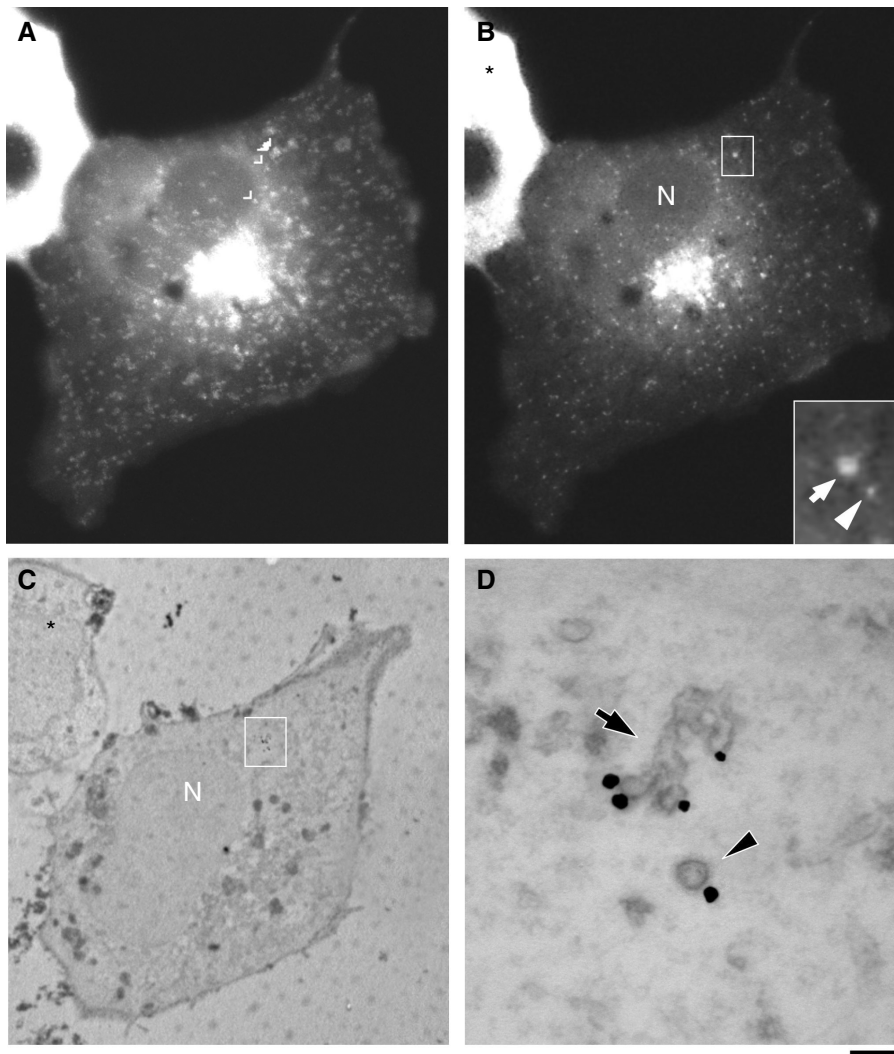


Figure 6: CLEM of clathrin-GFP-containing TCs. (A) HeLa cells were transfected with a plasmid encoding clathrin-light-chain-GFP and observed using confocal fluorescence microscopy. Projection of 33 time frames shows the trajectory of a clathrin-GFP-containing TC (indicated by arrowheads) moving from the TGN to the cell periphery. (B) The box and corresponding inset show the same clathrin-GFP-containing TC (arrow) just before fixation. Notice its location near the nucleus (N) and a neighboring compact structure (arrowhead). The asterisk indicates a cell that overexpresses clathrin-GFP. (C) Low magnification EM of the cell shown in A and B. The white box shows the location of the same clathrin-GFP-containing TC near the nucleus. As in panel B, the asterisk indicates the neighboring cell. (D) High magnification EM corresponding to inset in B and boxes in B, C. Arrow indicates the clathrin-GFP-containing TC located close to a typical CCV (arrowhead). Bar, 5.2 μm (A, B), 3.1 μm (C), 300 nm (D).

these TCs resemble, at least superficially, those of other long-range TCs such as ER-to-Golgi 'VTCs' (14,17,25) and TGN-to-plasma membrane carriers (12,13).

It is currently unclear whether TGN-to-endosome TCs undergo structural changes during their translocation through the cytoplasm. The apparent size and labeling intensity of the TCs did not seem to change during translocation. In addition, we did not observe budding of CCVs from the translocating TCs (9; this study). Instead, GFP-GGA1-containing TCs were observed to merge seemingly unchanged with rhodamine-albumin-loaded endosomes

(9). This indicates that (i) the TCs maintain their overall structure throughout their lifespan and (ii) at least GGA1 and clathrin remain associated with the TCs until the endosome-docking step. The persistence of the coats on the TCs could enable coupling of clathrin adaptors to microtubule motors (26) or fusion factors (27,28), thus contributing to the postbudding fate of the carriers as they transit toward the peripheral endosomes.

We have directly demonstrated that TGN-derived TCs deliver MPR-GFP into selectively bleached endosomes (see Figure 7A) and, hence, act as bona fide transport

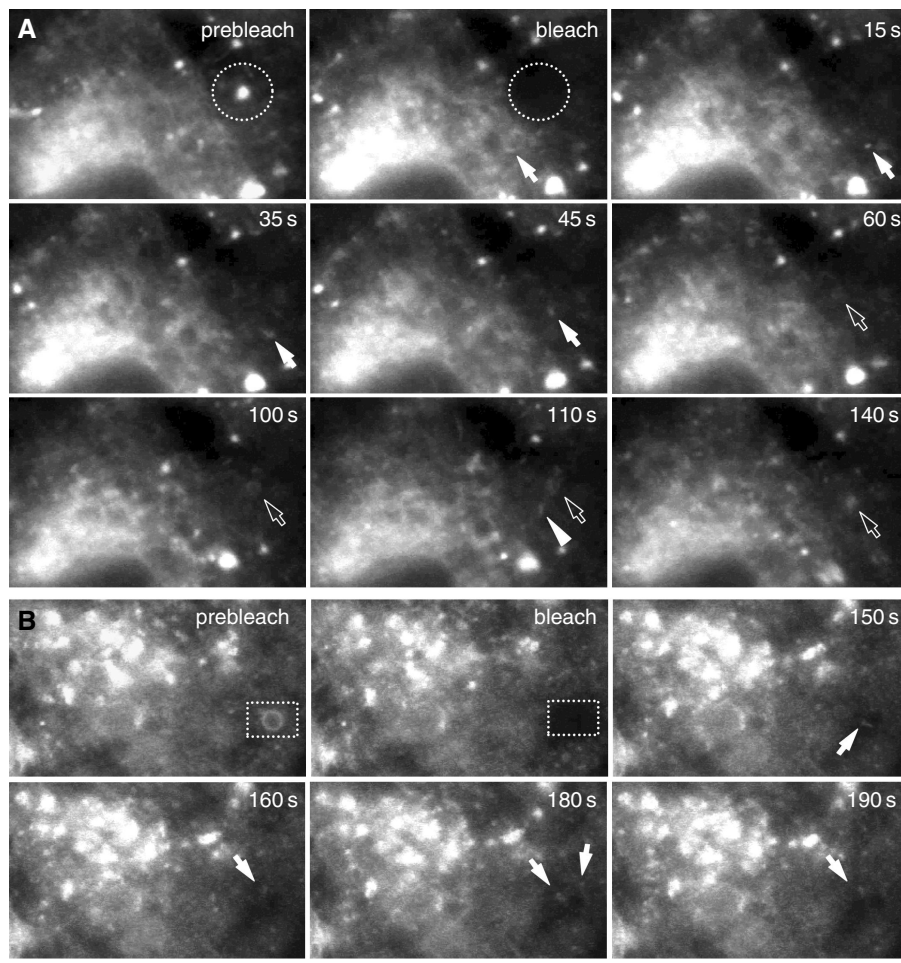


Figure 7: Inactivation of endosomes prevents their fusion with MPR-GFP-containing TCs. (A) HeLa cells expressing MPR-GFP were subjected to selective photobleaching within the area (dashed circle) containing an endosome (see Movie 6). Time-lapse images show an MPR-GFP-containing TC that moved from the TGN toward bleached area. It subsequently merged with the bleached endosome, resulting in partial recovery of fluorescence (open arrowhead). Fusion of other TCs (one of them is indicated by arrowheads) resulted in further recovery of the fluorescence within the same endosome (open arrow). (B) HeLa cells were transfected with a plasmid encoding MPR-GFP and incubated in HRP-containing medium for 1 h. The cells were then washed and placed in an ice-cold mixture of DAB and H_2O_2 to inactivate endosomes. The cells were then washed and observed *in vivo* at 37 °C. An endosome was bleached (dashed box) within an MPR-GFP-expressing cell (see Movie 7). Sequential time-lapse frames demonstrate that TCs (arrows) approached the bleached endosome but did not deliver MPR-GFP into it (notice the absence of fluorescence recovery in the bleached structure). Bar, 3.1 μ m (A, B).

intermediates in the TGN-to-endosome route. CLEM of some large TCs that were fortuitously caught in proximity to endosomes (Figure 5) revealed that they contained clathrin-coated membrane domains that were linked to one another by tubular connections. However, even using CLEM, it was difficult to observe a sufficiently large number of TCs that were docked to endosomes for detailed ultrastructural analysis. Thus, to examine TCs at the last stages of their life span, we blocked their fusion with target membranes using the technique of endosome inactivation (21–23). Under these conditions, TCs gathered around endosomes and were easily discernible in both plastic and cryo sections (Figure 8). Interestingly, their overall morphology was similar to that of TCs that were visualized using CLEM just after their detachment from

the TGN. Notably, the number of CCVs relative to large TCs did not change significantly as the carriers translocated through the cytoplasm. This suggests that large carriers do not break down into CCVs *en route* to peripheral endosomes. Coated domains were also maintained on the surface of the TCs that were arrested before fusion. The ultimate fate of these coated domains remains unclear. Presumably, they could lose their coat during fusion or, alternatively, they could become integrated into the endosome membrane.

Although pleiomorphic carriers represent significant part of TC population, at present, we do not know whether they operate exclusively in long-range TGN-to-endosome transport. This is because our methods do not allow us to

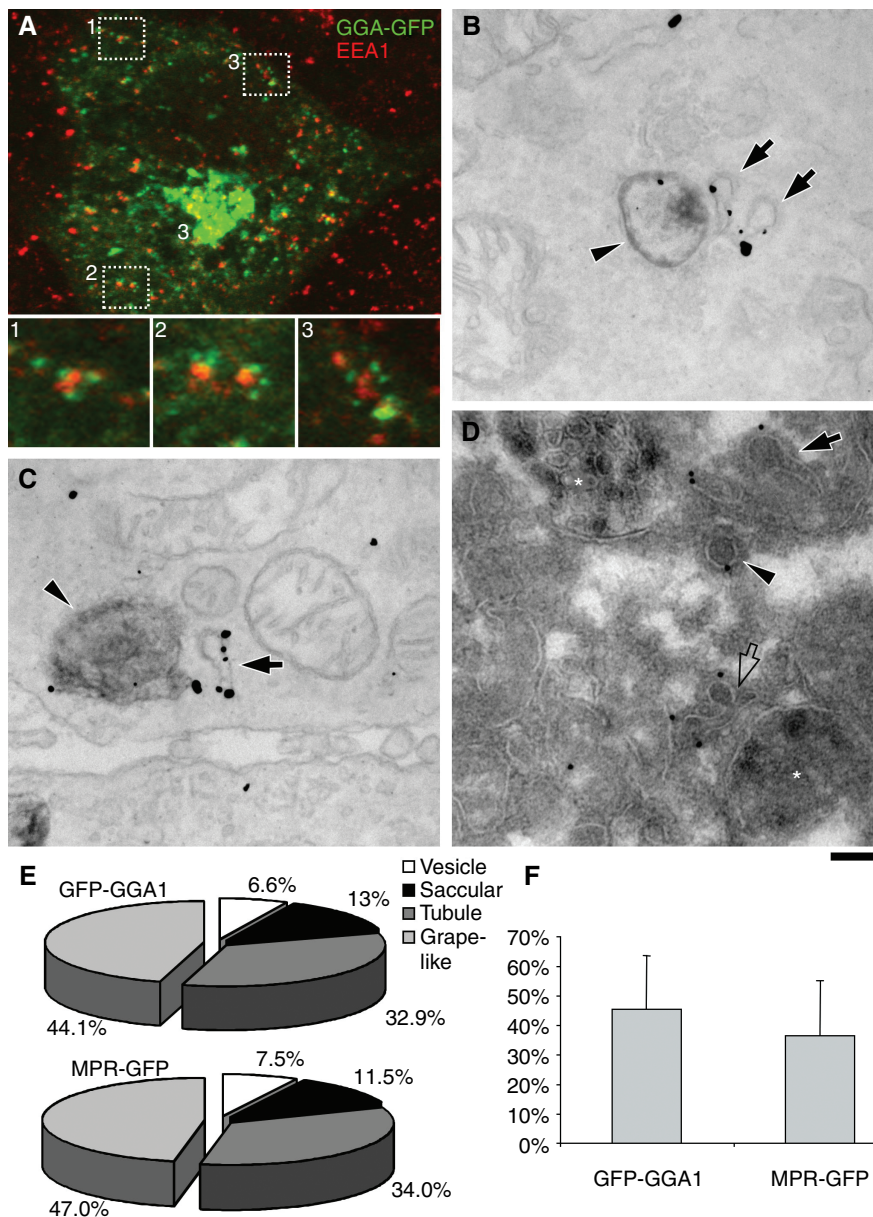


Figure 8: Ultrastructure of TGN-derived TCs visualized upon endosome inactivation. HeLa cells were transfected with a plasmid encoding either GFP-GGA1 (A–C) or clathrin-GFP (D) and incubated in HRP-containing medium for 1 h. The cells were then washed and placed in an ice-cold mixture of DAB and H₂O₂ to inactivate endosomes. The cells were subsequently shifted to 37 °C for 45 min and fixed and processed for either confocal (A) or electron (B–D) microscopy. For confocal microscopy, cells were labeled with anti-EEA1 antibody (A) to visualize endocytic structures, whereas immunogold EM was performed with anti-GFP antibody (B–D) using a preembedding protocol (B, C) or cryosections (D). (A) GFP-GGA1-containing TCs frequently accumulated around endosomal structures labeled for EEA1 (see boxes and corresponding insets) in cells with endosomes that were inactivated by DAB treatment. (B, C) Immunogold labeling with antibody to GFP revealed the ultrastructure of GFP-GGA1-containing TCs (arrows) located close to endosomes containing electron dense DAB product (arrowheads). (D) Clathrin-GFP-positive TCs of tubular (arrow), vesicular (arrowhead), and grape-like (open arrow) shapes were detected near endosomes (asterisks) and exhibited patches of electron-dense HRP labeling. (E) Pie charts representing the frequency of different shapes in populations of GFP-GGA1- and MPR-GFP-containing TCs observed upon endosome inactivation. (F) Percentage of area occupied by clathrin coat on the surface of GFP-GGA1- and MPR-GFP-containing TCs. Results are the mean \pm SD from 24 and 23 TCs, respectively. Bar, 7.2 μ m (A), 250 nm (B, C), 180 nm (B, C).

observe *in vivo* TCs in the juxtannuclear area of the cell, where TGN and some endosomes are located too close to each other. Short-range transfer of cargo between these

neighboring organelles could very well be mediated by conventional CCVs. In any event, our observations do demonstrate the existence of new and ultrastructurally

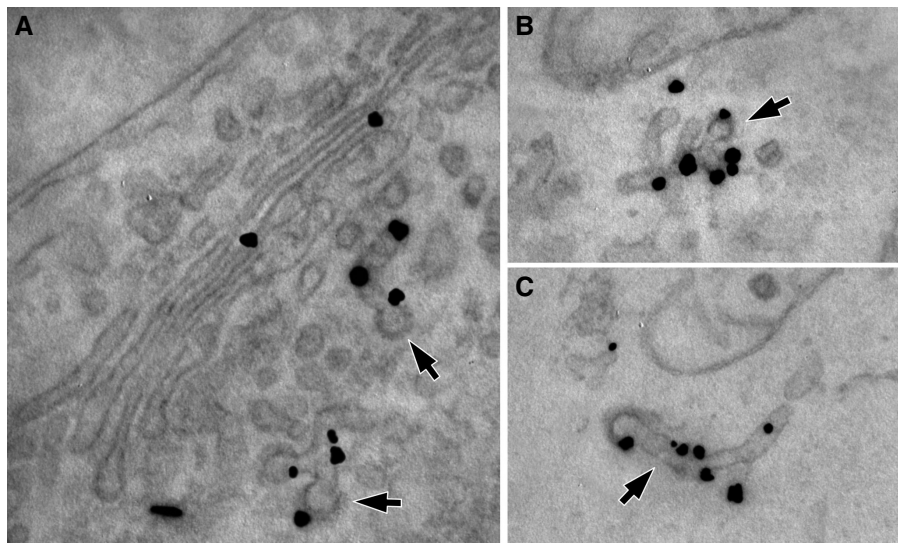


Figure 9: Ultrastructure of clathrin-coated domains at the TGN is reminiscent of the morphology of TCs. HeLa cells were transfected with a plasmid encoding MPR-GFP, fixed, stained with antibody to GFP using an immunogold protocol, and prepared for EM. (A) Arrows show clathrin-coated domains of the TGN containing MPR-GFP. (B, C) Free TCs (arrows) with MPR-GFP exhibit a morphology similar to that of TGN clathrin-coated domains (shown by arrows in A). Bar, 200 nm (A, C), 230 nm (B).

distinct type of clathrin-coated carrier involved in transport in Golgi-to-endosome route.

Materials and Methods

Cell culture and transfection

HeLa cells were cultured in DMEM (Gibco, Invitrogen SRL, Milan, Italy) supplemented with 10% fetal bovine serum and 1 mM L-glutamine. FuGENE 6 reagent (Roche, Indianapolis, IN, USA) or Lipofectamine 2000 (Invitrogen, Carlsbad, CA, USA) was used for cDNA transfections of sub-confluent cells.

Antibodies, DNA, and other reagents

Plasmids encoding CD-MPR-GFP, GFP-GGA1, and clathrin-light-chain-GFP were described previously (8,9). Polyclonal antibodies to GFP and EEA1 were from Abcam (Cambridge, UK). HRP was from Pierce (Rockford, IL, USA). AlexaTM 546-IgG and TRITC-dextran conjugates were from Molecular Probes (Leiden, the Netherlands). The NANOGOLD[®] gold – Ab conjugates and the GOLDENHANCETM EM kit were from Nanoprobes (Yaphank, NY USA).

Endosome inactivation

Cells were incubated with 10 µg/mL HRP in culture medium for 1 h, washed once in serum-free DMEM, and then twice in ice-cold PBS. Surface-bound HRP was removed by two 5-min washes in 0.15 M NaCl and 20 mM citric acid, pH 5.0. Cells were washed with ice-cold PBS, pH 7.4, and incubated in PBS containing 0.1 mg/mL DAB (Sigma-Aldrich, St Louis, MO, USA). H₂O₂ was added to the inactivation sample to a final concentration of 0.025%; PBS was added to the control set. Cells were incubated on ice for 60 min in the dark, and the reaction was stopped by washing cells twice in PBS/1% BSA. Warm medium was added, and cells were incubated at 37 °C for 45 min, fixed, and processed for either confocal or immuno-EM.

Confocal microscopy

Confocal and time-lapse images were obtained using a Zeiss LSM510 META confocal microscope system (Carl Zeiss, Göttingen, Germany) as described (13). Images of live cells were acquired using excitation at 488 nm and appropriate band filters. Fixed cells labeled with antibodies and/or fluorescent proteins were visualized using multitrack configuration with sequential excitation at 488 and 543 nm.

Immuno-EM and CLEM analysis

Fixation and immunogold detection of fluorescent proteins for EM was performed using antibody to GFP as described (13). After immunolabeling, cells were embedded in Epon-812 and cut into thin sections. CLEM of cells co-transfected with GFP constructs was performed as described (13). Briefly, transfected cells were grown on Petri dishes with CELLocate coverslips (Mat Tek, Ashland, MA, USA). After visualization of fluorescent structures by confocal microscopy, we fixed the cells, immuno-labeled for GFP using the GOLDENHANCE protocol, embedded in Epon-812, and cut into serial sections. Cryoimmuno EM was performed as described previously (29). A Philips Tecnai-12 electron microscope (Philips, Eindhoven, the Netherlands), equipped with ULTRA VIEW CCD digital camera, was used to acquire EM images. Three-dimensional reconstructions of structures observed in serial sections were reconstructed using SURFdriver software.

Acknowledgments

We thank E. Fontana for assistance with manuscript preparation. We acknowledge financial support from Telethon Italy (grants GPP05044 and GFT03006) and the Intramural Program of the NICHD, National Institutes of Health.

Supplementary Material

Movie 1: GFP-GGA1-containing TCs in living cells. HeLa cells were transfected with a plasmid-encoding GFP-GGA1 and imaged using confocal fluorescence microscopy. Three TCs (arrows) were observed to move from the juxtannuclear area, then fixed and processed for electron microscopy

(see Figure 1A–C). Note the apparent pleiomorphy of the GFP-GGA1-containing TCs.

Movie 2: Exit of GFP-GGA1-containing TCs from the Golgi. HeLa cells expressing GFP-GGA1 were observed under confocal microscope. Two GFP-GGA1-containing TCs (outlined by circle) were observed to exit the Golgi and were fixed shortly after formation for electron microscopy (Figure 1D–G).

Movie 3: MPR-GFP-containing TCs in living cells. HeLa cells were transfected with a plasmid encoding MPR-GFP and imaged using confocal fluorescence microscopy. Two TCs (arrows) were observed to move from the Golgi area to cell periphery, then fixed and processed for electron microscopy (Figure 2A–F).

Movie 4: Movement of MPR-GFP-containing TCs toward endosome. An MPR-GFP-expressing HeLa cell was analyzed under confocal microscopy. An MPR-GFP-containing TC (arrow) was observed to move from the Golgi toward endosome exhibiting circle-like pattern of fluorescent signal. TC was fixed before its fusion with endosome and processed for electron microscopy (Figure 2G,H).

Movie 5: Clathrin-GFP-containing TCs in living cells. HeLa cells were transfected with a plasmid encoding clathrin-GFP and visualized using confocal microscopy. A TCs (arrows) containing clathrin-GFP was observed during its movement from the Golgi to the peripheral portion of the cell, then fixed and processed for EM (Figure 3).

Movie 6: Delivery of MPR-GFP from the Golgi to endosome. HeLa cells expressing MPR-GFP were subjected to selective photobleaching within the area (circle) containing an endosome. Time-lapse images show an MPR-GFP-containing TC (arrow) that moved from the TGN toward bleached area. It subsequently merged with the bleached endosome, resulting in partial recovery of fluorescence (doubled arrow). Fusion of other TCs (arrow) resulted in further recovery of the fluorescence within the same endosome.

Movie 7: Inactivation of endosomes prevents their fusion with MPR-GFP-containing TCs. HeLa cells were transfected with a plasmid encoding MPR-GFP and incubated in HRP-containing medium for 1 h. The cells were then washed and placed in an ice-cold mixture of DAB and H₂O₂ to inactivate endosomes. The cells were then washed and observed *in vivo* at 37 °C. An endosome was bleached (box) within an MPR-GFP-expressing cell. Time-lapse sequence demonstrate that TCs approached the bleached endosome but did not deliver MPR-GFP into it (notice the absence of fluorescence recovery in the bleached structure).

These materials are available as part of the online article from <http://www.blackwell-synergy.com>

References

- Ghosh P, Dahms NM, Kornfeld S. Mannose 6-phosphate receptors: new twists in the tale. *Nat Rev Mol Cell Biol* 2003;4:202–212.
- Geuze HJ, Slot JW, Strous GJ, Hasilik A, von Figura K. Possible pathways for lysosomal enzyme delivery. *J Cell Biol* 1985;101:2253–2262.
- Klumperman J, Hille A, Veenendaal T, Oorschot V, Stoorvogel W, von Figura K, Geuze HJ. Differences in the endosomal distributions of the two mannose 6-phosphate receptors. *J Cell Biol* 1993;121:997–1010.
- Doray B, Ghosh P, Griffith J, Geuze HJ, Kornfeld S. Cooperation of GGAs and AP-1 in packaging MPRs at the *trans*-Golgi network. *Science* 2002;297:1700–1703.
- Campbell CH, Rome LH. Coated vesicles from rat liver and calf brain contain lysosomal enzymes bound to mannose 6-phosphate receptors. *J Biol Chem* 1983;258:13347–13352.
- Sahagian GG, Steer CJ. Transmembrane orientation of the mannose 6-phosphate receptor in isolated clathrin-coated vesicles. *J Biol Chem* 1985;260:9838–9842.
- Huang F, Nesterov A, Carter RE, Sorkin A. Trafficking of yellow-fluorescent-protein-tagged mu1 subunit of clathrin adaptor AP-1 complex in living cells. *Traffic* 2001;2:345–357.
- Puertollano R, Aguilar RC, Gorshkova I, Crouch RJ, Bonifacino JS. Sorting of mannose 6-phosphate receptors mediated by the GGAs. *Science* 2001;292:1712–1716.
- Puertollano R, van der Wel NN, Greene LE, Eisenberg E, Peters PJ, Bonifacino JS. Morphology and dynamics of clathrin/GGA1-coated carriers budding from the *trans*-Golgi network. *Mol Biol Cell* 2003;14:1545–1557.
- Waguri S, Dewitte F, Le Borgne R, Rouille Y, Uchiyama Y, Dubremetz JF, Hoflack B. Visualization of TGN to endosome trafficking through fluorescently labeled MPR and AP-1 in living cells. *Mol Biol Cell* 2003;14:142–155.
- Mironov AA, Polishchuk RS, Luini A. Visualizing membrane traffic *in vivo* by combined video fluorescence and 3D electron microscopy. *Trends Cell Biol* 2000;10:349–353.
- Polishchuk RS, Polishchuk EV, Marra P, Alberti S, Buccione R, Luini A, Mironov AA. Correlative light-electron microscopy reveals the tubular-saccular ultrastructure of carriers operating between Golgi apparatus and plasma membrane. *J Cell Biol* 2000;148:45–58.
- Polishchuk EV, Di Pentima A, Luini A, Polishchuk RS. Mechanism of constitutive export from the golgi: bulk flow via the formation, protrusion, and *en bloc* cleavage of large *trans*-Golgi network tubular domains. *Mol Biol Cell* 2003;14:4470–4485.
- Mironov AA, Mironov AA Jr, Beznoussenko GV, Trucco A, Lupetti P, Smith JD, Geerts WJ, Koster AJ, Burger KN, Martone ME, Deerink TJ, Ellisman MH, Luini A. ER-to-Golgi carriers arise through direct *en bloc* protrusion and multistage maturation of specialized ER exit domains. *Dev Cell* 2003;5:583–594.
- Arighi CN, Hartnell LM, Aguilar RC, Haft CR, Bonifacino JS. Role of the mammalian retromer in sorting of the cation-independent mannose 6-phosphate receptor. *J Cell Biol* 2004;165:123–133.
- Carlton J, Bujny M, Peter BJ, Oorschot VM, Rutherford A, Mellor H, Klumperman J, McMahon HT, Cullen PJ. Sorting nexin-1 mediates tubular endosome-to-TGN transport through coincidence sensing of high-curvature membranes and 3-phosphoinositides. *Curr Biol* 2004;14:1791–1800.
- Martinez-Menarguez JA, Geuze HJ, Slot JW, Klumperman J. Vesicular tubular clusters between the ER and Golgi mediate concentration of soluble secretory proteins by exclusion from COPI-coated vesicles. *Cell* 1999;98:81–90.
- Horstmann H, Ng CP, Tang BL, Hong W. Ultrastructural characterization of endoplasmic reticulum – Golgi transport containers (EGTC). *J Cell Sci* 2002;115:4263–4273.
- Klumperman J, Kuliawat R, Griffith JM, Geuze HJ, Arvan P. Mannose 6-phosphate receptors are sorted from immature secretory granules via adaptor protein AP-1, clathrin, and syntaxin 6-positive vesicles. *J Cell Biol* 1998;141:359–371.
- Dittie AS, Klumperman J, Tooze SA. Differential distribution of mannose-6-phosphate receptors and furin in immature secretory granules. *J Cell Sci* 1999;112:3955–3966.
- Stoorvogel W, Geuze HJ, Griffith JM, Strous GJ. The pathways of endocytosed transferrin and secretory protein are connected in the *trans*-Golgi reticulum. *J Cell Biol* 1988;106:1821–1829.
- Futter CE, Connolly CN, Cutler DF, Hopkins CR. Newly synthesized transferrin receptors can be detected in the endosome before they appear on the cell surface. *J Biol Chem* 1995;270:10999–11003.
- Ang AL, Taguchi T, Francis S, Folsch H, Murrells LJ, Pypaert M, Warren G, Mellman I. Recycling endosomes can serve as

- intermediates during transport from the Golgi to the plasma membrane of MDCK cells. *J Cell Biol* 2004;167:531–543.
24. Orci L, Malhotra V, Amherdt M, Serafini T, Rothman JE. Dissection of a single round of vesicular transport: sequential intermediates for intercisternal movement in the Golgi stack. *Cell* 1989;56:357–368.
 25. Bannykh SI, Rowe T, Balch WE. The organization of endoplasmic reticulum export complexes. *J Cell Biol* 1996;135:19–35.
 26. Nakagawa T, Setou M, Seog D, Ogasawara K, Dohmae N, Takio K, Hirokawa N. A novel motor, KIF13A, transports mannose-6-phosphate receptor to plasma membrane through direct interaction with AP-1 complex. *Cell* 2000;103:569–581.
 27. Shiba Y, Takatsu H, Shin HW, Nakayama K. Gamma-adaptin interacts directly with Rabaptin-5 through its ear domain. *J Biochem (Tokyo)* 2002;131:327–336.
 28. Mattera R, Arighi CN, Lodge R, Zerial M, Bonifacino JS. Divalent interaction of the GGAs with the Rabaptin-5-Rabex-5 complex. *EMBO J* 2003;22:78–88.
 29. Peters P. Cryoimmunogold electron microscopy. In: Bonifacino JS, Dasso M, Harford JB, Lippincott-Schwartz J, Yamada KM, editors. *Current Protocols in Cell Biology*. New York: John Wiley & Sons; 2001, 4.8.1–4.8.9.